Robust Stacking-Independent Ultrafast Charge Transfer in MoS₂/WS₂ Bilayers

Ziheng Ji,[†,∇] Hao Hong,[†,∇] Jin Zhang,[‡,∇] Qi Zhang,[§,∇] Wei Huang,[∥] Ting Cao,[⊥] Ruixi Qiao,[†] Can Liu,[†] Jing Liang,[†] Chuanhong Jin,[*,∥] Liying Jiao,[§] Kebin Shi,[*,†,#] Sheng Meng,[‡,#] and Kaihui Liu[*,†,#]

[†]State Key Laboratory for Mesoscopic Physics, School of Physics, Peking University, Beijing 100871, China

[‡]Beijing National Laboratory for Condensed Matter Physics, and Institute of Physics, Chinese Academy of Sciences, Beijing 100190, China

[§]Key Laboratory of Organic Optoelectronics and Molecular Engineering of the Ministry of Education, Department of Chemistry, Tsinghua University, Beijing 100084, China

[∥]State Key Laboratory of Silicon Materials, Key Laboratory of Advanced Materials and Applications for Batteries of Zhejiang Province, School of Materials Science and Engineering, Zhejiang University, Hangzhou, Zhejiang 310027, China

[⊥]Department of Physics, University of California at Berkeley, Berkeley, California 94720, United States

[#]Collaborative Innovation Centre of Quantum Matter, Beijing 100871, China

Ⓢ *Supporting Information*

ABSTRACT: Van der Waals-coupled two-dimensional (2D) heterostructures have attracted great attention recently due to their high potential in the next-generation photodetectors and solar cells. The understanding of charge-transfer process between adjacent atomic layers is the key to design optimal devices as it directly determines the fundamental response speed and photon-electron conversion efficiency. However, general belief and theoretical studies have shown that the charge transfer behavior depends sensitively on interlayer configurations, which is difficult to control accurately, bringing great uncertainties in device designing. Here we investigate the ultrafast dynamics of interlayer charge transfer in a prototype heterostructure, the MoS₂/WS₂ bilayer with various stacking configurations, by optical two-color ultrafast pump−probe spectroscopy. Surprisingly, we found that the charge transfer is robust against varying interlayer twist angles and interlayer coupling strength, in time scale of ∼90 fs. Our observation, together with atomic-resolved transmission electron characterization and time-dependent density functional theory simulations, reveals that the robust ultrafast charge transfer is attributed to the heterogeneous interlayer stretching/sliding, which provides additional channels for efficient charge transfer previously unknown. Our results elucidate the origin of transfer rate robustness against interlayer stacking configurations in optical devices based on 2D heterostructures, facilitating their applications in ultrafast and high-efficient optoelectronic and photovoltaic devices in the near future.

KEYWORDS: 2D heterostructures, stacking configuration, van der Waals coupling, robust ultrafast charge transfer, time-dependent density functional theory
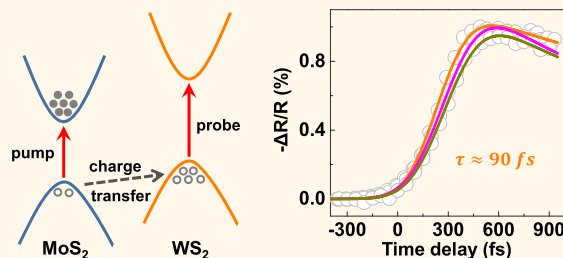
The family of two-dimensional (2D) materials, ranging from semimetallic graphene and infrared-gapped black phosphorus to semiconducting molybdenum disulfide (MoS₂) and insulating hexagonal boron nitride (h-BN), have demonstrated distinct electronic, optical and mechanical properties from conventional bulk materials. Stacking different 2D materials vertically leads to van der Waals heterostructures, which have emerged as a new class of materials and opened up significant opportunities for exploring novel physics and device applications.[1−5] Among various van der Waals heterostructures, those formed by two different transition-metal dichalcogenides (MX₂) monolayers are especially intriguing because of their giant tunability of bandgap size from infrared to visible range

and enhanced light-matter interaction.[6,7] Moreover, many MX₂ heterostructures form type II band alignment, indicating the photoexcited electrons and holes naturally separate into the two different layers through charge transfer process.[8−11] Despite the large interlayer momentum mismatch and the weak interlayer coupling between layers, which usually hinders the charge transfer process, both experiments[12−16] and theoretical calculations[17−20] elucidate that this process is ultrafast, and happens in a time scale of 100 fs. Several mechanisms for the

charge transfer, such as exciton localization,[17] interlayer hot excitons formation,[14,17] and coherent charge transfer,[15,18] have been proposed, while a comprehensive understanding is still lacking so far.

Interfacial stacking configuration is demonstrated to be an efficient degree of freedom to engineer the physical properties of van der Waals-coupled materials, e.g., interfacial states and wave function coupling.[21,22] Therefore, how the charge-transfer time evolves with the interfacial stacking configuration is both fundamental and important for understanding the interlayer charge transfer and optimizing applications of 2D hetero-structures. Several groups have reported the charge transfer time is ultrafast in tens femtosecond time scale regardless of different interlayer twist angle and thus different interlayer momentum mismatch.[12,13,16] Their experiments are all based on transferred MX_2 heterostructures with random twisted angle ($0° < \theta < 60°$), which have relatively weak and constant coupling strengths. Theoretical calculations indicate the charge transfer time could be different by 1 order of magnitude when lattice aligns into highly symmetric interfacial stacking configuration (e.g., perfectly 0° and 60° stacking),[19,20] while how it evolves experimentally still remains elusive due to the complex environment (e.g., strain, lattice mismatch) in realistic heterostructure interfaces.

In this article, we experimentally investigate the interlayer charge transfer process in as-grown MoS_2/WS_2 bilayers with multiple interlayer twist configurations. We find that while the interlayer mechanical coupling varies with interlayer twist angles, the interlayer charger transfer is surprisingly fast (~100 fs) and remains nearly constant for all configurations studied. Further atomic resolved characterization and ab initio calculations reveal that local stacking inhomogeneity (stretching/sliding) exist in our as-grown materials, and the inhomogeneity provides multichannels for the charge transfer. The fastest channel dominates the measurable charge transfer time and leads to the robust ultrafast behavior against varying stacking configurations.

RESULTS AND DISCUSSION

Geometric Configuration of Twisted MoS_2/WS_2 Bilayers. In our experiment, high quality MoS_2/WS_2 bilayers were grown on 90 nm SiO_2/Si substrates by chemical vapor deposition (CVD) method.[23−25] Using core−shell $WO_{3−x}/MoO_{3−x}$ nanowires as a precursor to ensure the sequential growth of MoS_2 and WS_2, pristine MoS_2/WS_2 bilayers were successfully grown with different interlayer twist angle.[23] Figure 1a−c show, respectively, optical reflection images of MoS_2/WS_2 bilayers with twist angle of $\theta = 0°$, 60°, and 38°. The smaller top layer is WS_2 monolayer and the larger bottom one is MoS_2 monolayer. Raman spectra confirm that the overlapping area are vertical heterostructures constituted of MoS_2 and WS_2 monolayers (Supplementary Figure S1a). The twist angle between layers can be directly obtained according to their relative geometry, because the orientation of each triangle is directly correlated with its microscopic crystal orientation.[26,27] To further built the relationship between twist angle and staking order, second-harmonic generation (SHG) was applied on the bilayers (Supplementary Figure S1b): similar to homogeneous bilayers, $\theta = 0°$ (60°) bilayers correspond to AA (AB) stacking.[21]

Interlayer Electronic and Mechanical Coupling in MoS_2/WS_2 Bilayers. Excited by 532 nm laser at room temperature, MoS_2/WS_2 bilayers show two pronounced peaks
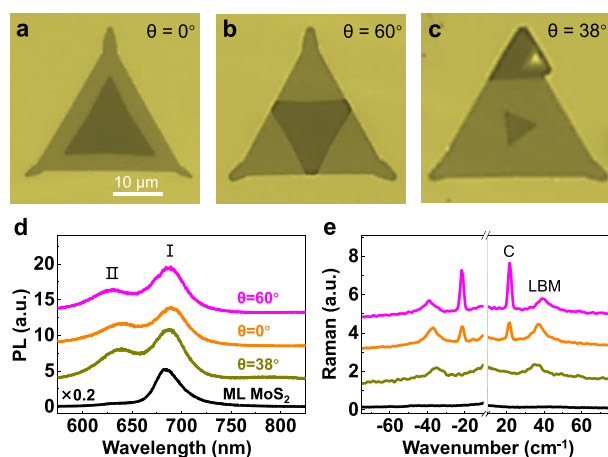

Figure 1. Twist-dependent interlayer coupling in MoS_2/WS_2 bilayers. (a−c) Optical images of CVD grown MoS_2/WS_2 bilayers with different twist angle. The small top triangle layer corresponds to a WS_2 monolayer, while the bottom large triangle layer corresponds to a MoS_2 monolayer. Scale bar is 10 μm. (d) Photoluminescence of MoS_2 monolayer and MoS_2/WS_2 bilayers. The two obvious peaks in heterostructures corresponds to direct A-exciton transitions from MoS_2 (peak I) and WS_2 (peak II), respectively. Intensity of Peak I in heterostructures are about 1/5 of that in MoS_2 monolayer, indicating strong interlayer electronic coupling and efficient electron−hole separation. (e) Low-frequency Raman spectra of MoS_2 monolayer and heterostructures with different twist angles corresponding to a−c. Higher LBM frequency indicates stronger mechanical coupling strength.

around 686 and 637 nm in the photoluminescence (PL) spectra (Figure 1d), which correspond to A-excitons of MoS_2 and WS_2, respectively. PL is strongly quenched (by ~5 times) in MoS_2/WS_2 bilayers compared to MoS_2 monolayers. This reduced PL signals in bilayer indicate strong electronic coupling between MoS_2 and WS_2 monolayers and hint at the efficient interlayer charge transfer.[12−15]

Interlayer coupling can also significantly modify the phonon vibrations in atomic-layered materials, especially the low-energy interlayer vibration modes.[28−32] We utilized Raman spectroscopy to study the interlayer coupling strength. Figure 1e shows the low-frequency Raman spectra of MoS_2/WS_2 bilayers with twist angle of $\theta = 0°$, 60°, and 38°. Two pronounced peaks in the range of 20−40 cm^{-1}, corresponding to the in-plane shear (C) mode and the out-of-plane layer breathing mode (LBM), are observed.[25] Linearly polarized Raman measurement with parallel and cross-polarization configurations was also measured to further clarify the shear and breathing modes of MoS_2/WS_2 bilayers (Supplementary Figure S2).[28,31] LBM can reflect interlayer mechanical coupling strength: the higher the LBM frequency, the stronger the interlayer mechanical coupling strength. From our experimental results, AB and AA stacking bilayers have stronger mechanical coupling than the randomly twisted one.

The C mode is clearly observed in AA and AB stacking but disappears in the twist configurations. This is because AA and AB staking are energetically favorable staking configurations, so that lateral displacement can provide a tangent restoring force, while the force is unattainable in the twist configuration.[30,32] The clear C mode signal also reflects that crystallographic structures of MoS_2 and WS_2 monolayers are nicely aligned in our AA/AB stacking bilayers. For comparison, MoS_2 monolayers have no significant Raman peaks around 30 cm^{-1}.

Ultrafast Charge Transfer Dynamics in MoS$_2$/WS$_2$ Bilayers. Typically, MoS$_2$/WS$_2$ bilayers form the type II heterojunctions: the conduction band minimum (CBM) and valence band maximum (VBM) reside at MoS$_2$ and WS$_2$ layers, respectively (Figure 2b).[8,9] After photoexcitation of MoS$_2$,
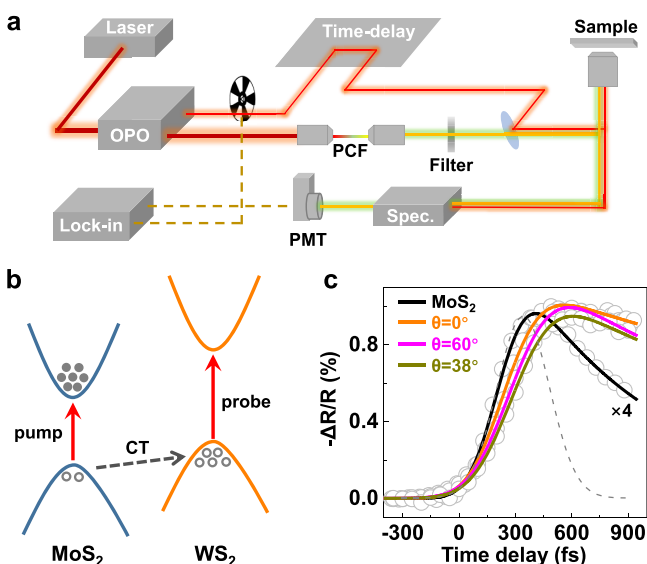

Figure 2. Ultrafast charge transfer dynamics in MoS$_2$/WS$_2$ bilayers. (a) Schematics of the optical two-color pump−probe setup. (b) Band alignment of MoS$_2$/WS$_2$ bilayers. After optically pumping MoS$_2$ A-exciton, the hole will transfer to a lower energy at WS$_2$ while the electron remains in MoS$_2$, leading to an efficient electron−hole separation and interlayer exciton formation. By selectively probing with a higher energy light at WS$_2$ A-exciton resonance, we get the transient absorption spectra of MoS$_2$/WS$_2$ bilayers reflecting the charge transfer dynamics, as shown in (c).

holes will transfer to a lower energy state at the VBM of WS$_2$ while the electrons still stay in MoS$_2$. To capture this charge transfer dynamics in MoS$_2$/WS$_2$ bilayers, we performed femtosecond pump−probe experiments at room temperature. Figure 2a shows schematically the optical ultrafast two-color pump−probe setup. Femtosecond pulses (∼100 fs, 80 MHz) at 820 nm were guided into an optical parametric oscillator

(OPO) to generate pump laser. The residue of 820 nm pulses were coupled into a section of photonic crystal fiber (PCF), then using optical filters and spectrometer to realize wavelength-tunable probing.

Using a pump fluence of 12 μJ/cm^2, we selectively excite MoS$_2$ by choosing the excitation energy at 1.73 eV. The pump energy is at the tail of MoS$_2$ A-exciton peak and far below the resonance absorption energy of WS$_2$ to avoid exciting WS$_2$. After the initial pump, higher photon energy pulses center at 1.95 eV (at the same energy as the WS$_2$ A-exciton and close to the MoS$_2$ B-exciton) are used as the probe.[12] The transient absorption spectra of MoS$_2$ monolayer and MoS$_2$/WS$_2$ bilayers with different twist angles are shown in Figure 2c. For monolayer MoS$_2$, the transient absorption signal is from MoS$_2$ B-exciton probing. Its curve rises instantaneously since the formation of B-exciton right after the pump pulse excitation.[12] While for MoS$_2$/WS$_2$ bilayers, the signals are about 4 times stronger than that for MoS$_2$ monolayers, indicating the signals are mostly from WS$_2$. In addition, the signals from MoS$_2$/WS$_2$ bilayers rise slightly slower than MoS$_2$ monolayer around time-zero since the signals of WS$_2$ probing arise after pump pulse excitation and interlayer charge transfer process. Since the pump energy is well below the B-exciton energy of MoS$_2$ (150 meV above A-exciton), the charge/energy transfer process between MoS$_2$ B-exciton states and WS$_2$ states can be excluded. Also, low energy pumping of MoS$_2$ A-exciton without exciting WS$_2$ avoid energy transfer between MoS$_2$ and WS$_2$.[33] Therefore, only hole transfer process from MoS$_2$ A-exciton states to WS$_2$ A-exciton states are allowed in the interlayer charge transfer process of our experiments. Interestingly, for MoS$_2$/WS$_2$ bilayers with different interlayer twist angles the rise times are only slightly varied, suggesting that the charge transfer time is robust and stacking independent, in striking contrast to the mechanical coupling. After deconvolution,[12] we confirm the charge transfer time in MoS$_2$/WS$_2$ bilayers is around 90 fs in all cases (as shown in Table 1). The instrument response function is shown as the gray dashed curve in Figure 2c. At room temperature, we characterized 10 CVD-grown samples and 2 transferred samples with different twist angles, their charge transfer times are all in time scale around 90 fs (Supplementary Figure S3). Experiments at temperature of 77 K show similar trends as well (Supplementary Figure S4). This robust ultrafast

Table 1. Mechanical Coupling and Charge Transfer (CT) in MoS$_2$/WS$_2$ Bilayers[a]

configuration	shear mode (cm^{-1})	breathing mode (cm^{-1})	CT-exp. (fs)	interlayer sliding (nm)	interlayer distance (nm)	CT-theory (fs)
$\theta = 0°$	21.4	37.5	84	0.00 (AA$_1$)	0.63	1500[20]
				0.02 (AA$'_1$)	0.63	102
				0.03 (AA$'_1$)	0.63	42
				0.05 (AA$'_1$)	0.63	5110
				0.06 (AA$'_1$)	0.63	847
				0.00 (AA$_3$)	0.68	180[20]
$\theta = 38°$	–	36.0	93	0	0.65	280
$\theta = 60°$	21.6	40.0	89	0.00 (AB$_1$)	0.63	150[20]
				0.02 (AB$'_1$)	0.63	725
				0.03 (AB$'_1$)	0.63	226
				0.06 (AB$_1'$)	0.63	245
				0.08 (AB$'_1$)	0.63	800
				0.00 (AB$_2$)	0.63	1050[20]

[a]AA$'_1$ and AB$'_1$ corresponding to AA$_1$ and AB$_1$ stacking with an interlayer sliding.

charge transfer behavior in MoS_2/WS_2 bilayers is also consistent with their almost identical PL yields (Figure 1d), since the PL quenching originates from the interlayer charge transfer. This observation is quite strange and disobeys the common sense that different twist angles give different interlayer momentum space rotations of valleys, and therefore led to different charge-transfer times (the charge transfer is highly dependent on specific interlayer states). In fact, previous theoretical calculations point out that AA, AB and twist configuration should have very different charge transfer time ranging from 100 fs to 1 ps scale.[19,20]

Atomic-Resolved Characterization on MoS_2/WS_2 Bilayers. To explore the underlying mechanism of the twist-angle independent charge transfer in MoS_2/WS_2 bilayers, we apply scanning transmission electron microscopic (STEM) characterization on our samples with atomic resolution. Figure 3a displays the typical STEM image of an AA-stacking MoS_2/
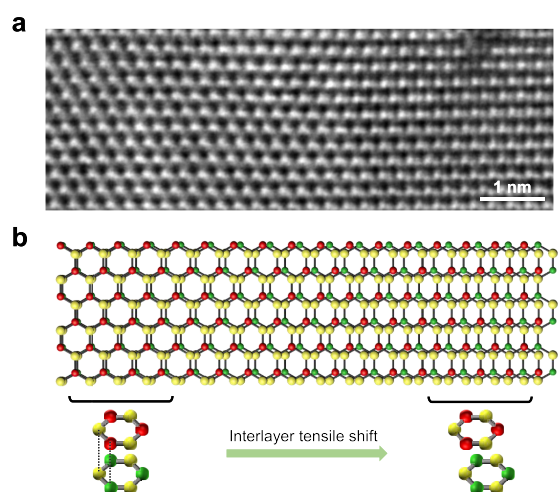
Figure 3. Atomic-resolved characterized of MoS_2/WS_2 bilayers by STEM. (a) STEM image of an AA-stacking MoS_2/WS_2 bilayers. At the left side of the image, MoS_2/WS_2 bilayer shows AA$_3$-stacking, a high-energy stacking pattern. While going over to the right side, an interlayer tensile shift appears and serves as transition region between two high-symmetric stacking configurations. The diagrammatic sketch is shown in (b).

WS_2 bilayer transferred on a holey carbon TEM grid. In principle, MX_2 bilayer and MX_2 heterostructures have six high-symmetry stacking configurations (Supplementary Figure S5).[21] STEM image indicates that, in addition to the energy-favorable AA$_1$ stacking, there exists high-energy state of AA$_3$ stacking, due to interlayer stretching and shifting (Figure 3b). This shifted interlayer stretching/shifting and coexistent multidomains are widely observed in 2D bilayer systems, such as MoS_2/WSe_2,[34] graphene/graphene[35,36] and graphene/ BN.[37] Its formation should be attributed to the local tensile strain during the CVD cooling process.[38] MoS_2/WS_2 bilayers are grown at 800 °C and then cooled down to room temperature. During high temperature growth, the slight lattice constant difference between MoS_2 and WS_2 will introduce local strain for two layer match together.[39] Then in the following cooling process, the local strain will be further amplified and bring interlayer shift due to their different thermal expansion coefficients.[40] We propose that the local structural inhomogeneity at atomics scale is the origin for the robustness of the ultrafast interlayer charge transfer.

First-Principle Calculations on Charge Transfer in MoS_2/WS_2 Bilayers. To quantitatively understand the robustness of the ultrafast charge transfer behavior, we performed time-dependent density function theory (TDDFT) calculations on different stackings of MoS_2/WS_2 bilayers.[41,42] Previous calculations only dealt with the perfectly stacked heterostructures with high-symmetry stacking configurations.[19,20] Here we calculate the charge transfer dynamics in the AA/AB stacking bilayer with interlayer tensile shift. Interlayer tensile shift between MoS_2 layer and WS_2 layer is described by an interlayer sliding (Figure 4a,b for AA and AB stackings,
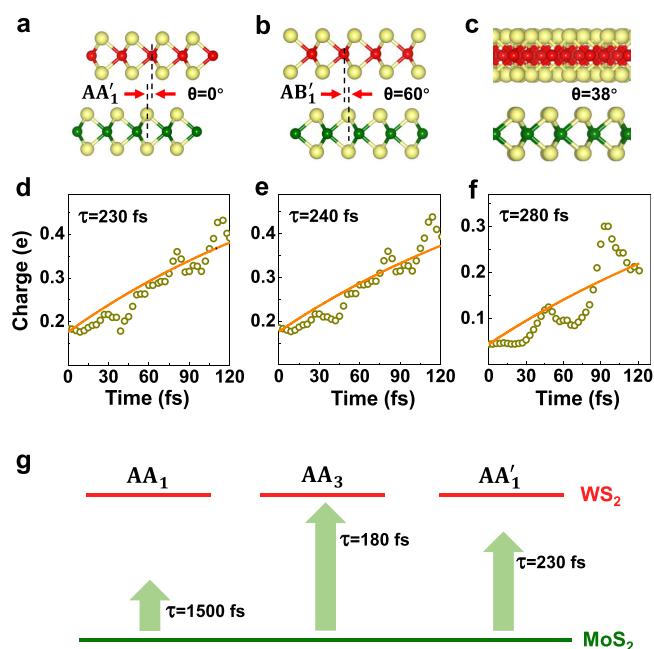
Figure 4. Theoretical understanding of robust ultrafast charge transfer in MoS_2/WS_2 bilayers. (a, b) Schematic atomic structures of the transition region in AA-/AB-stacking MoS_2/WS_2 bilayers, defined as AA′-/AB′-stacking. Interlayer tensile shift between MoS_2 layer and WS_2 layer is described by an interlayer sliding. Schematics of MoS_2/WS_2 bilayers with twist angle of 38° is shown in (c). (d−f) Evolutions of the hole transfer in the three stacking configurations corresponding to a−c. After the first photoexcitation at t = 0 fs, holes in MoS_2 will transfer to WS_2 in the following ~100 fs. The calculated integrals of excited hole density on WS_2 orbitals are fitted by an exponential curve to get the charge transfer time in different stacking configuration. (g) Schematic of charge transfer process across the heterogeneous interface of AA-stacking MoS_2/ WS_2 bilayers. The apparent transfer time is mainly determined by the fastest channel.

respectively). By artificially moving MoS_2 layer along the tangent direction from its most stable configuration with a random distance, we find the charge transfer time is much different from the perfectly aligned ones (Supplementary Figure S6). For each twist angle, charge transfer dynamics under four arbitrary interlayer shifts are calculated, summed then exponentially fitted to achieve the equivalent charge transfer time.

Figure 4d−f show TDDFT-calculated integral of excited holes density on WS_2 orbitals, which describe the charge transfer dynamics quantitatively. At t = 0, an electron is promoted from MoS_2 VBM to its CBM to simulate the first photoexcited state. Then in the following ~100 fs, the hole transfer process leads to hole localized on WS_2 layer. We found

the equivalent charge transfer times is around 250 fs across different twist angle (Figure 4d,e), in consistent with robustness we observed experimentally.

Charge transfer is determined by the specific electronic states, and various stacking modes provide multiple parallel channels in the charge transfer between the adjacent layers. The transfer time can be 1 order of magnitude different across different stacking configurations, but the measured apparent charge transfer time (Figure 4g) are mainly determined by the fastest channel, as the excited holes living near the slower channels could migrate and use faster channels. Take the AA stacking as an example, shown in Table 1, the hole transfer time is 1500 fs for AA_1 and 180 fs for AA_3, while the tensile one gives out 230 fs. Therefore, the charge transfer mainly happens at the AA_3 region. The situation is quite different for mechanical coupling measured by the Raman spectroscopy, which is determined by the second derivative of the potential energy of the system with respect to certain modes. As a result, the frequency of these modes can hardly be influenced by the local high-energy stacking regions. The interlayer force constant is mainly determined by the interlayer distance and registration due to steric effect, and therefore the LBM Raman frequencies of AA and AB stacked bilayers are always larger than randomly twisted ones.[21,25]

CONCLUSIONS

In conclusion, we have investigated the interlayer charge transfer in MoS_2/WS_2 bilayers with different stacking configurations. Although previous theoretical calculations predict that charge transfer is very sensitive to the interfacial configuration, in the as-grown materials the ultrafast charge transfer time is very robust. In addition to the hot excitons effect, we think the coexistence of various local stacking configurations and the associated parallel multichannels in the inhomogeneity interface is also one very important factor for twist angle independent ultrafast charge transfer. In the future device designing on 2D heterostructures for fast and high-efficiency optoelectronic and photovoltaic applications, our discovery of the multiple charge transfer channels eliminates the concerns on stacking-dependent effects, and allows for simple integration of one layer on the other. The formed heterostructures will have fast response speed and high charge transfer efficiency determined by the fastest channel.

METHODS

CVD Growth of MoS_2/WS_2 Vertical Heterostructures. The MoS_2/WS_2 vertical heterostructures with different twist angle were synthesized by CVD method.[23] The carbon fabric strip with WO_{3-x}/MoO_{3-x} core−shelled nanowires was directly placed on the top of 90 nm-thick SiO_2/Si substrate in the center of the furnace, and a ceramic boat with sulfur powder was placed upstream. After purging the system with Ar for 15 min, the furnace was heated up to 800 °C at a rate of 20 °C min^{-1}. When the temperature of furnace reached 800 °C, sulfur was heated by a heating belt with an individual temperature controller at ∼180 °C and then the furnace was cooled down naturally after staying at 800 °C for another 30 min. The heating belt for sulfur was removed when the furnace was cooled down to 400 °C.

Two-Color Pump−Probe Spectroscopy. Femtosecond pulses (∼100 fs) at 820 nm are generated by a Ti:sapphire 80 MHz oscillator then split into two path. One path of the light is used to pump an optical parametric oscillator (OPO) to generate wavelength tunable pump pulses, and the other path light is focused into a photonic crystal fiber (PCF) to generate a supercontinuum white light then pass through a filter (620−90X band-pass) to be used as probe pulses.

Those two pulses are separated in the time-domain by a controllable delay-time Δt and focused onto the sample. After collection of the reflected pulses and wavelength selection through a spectrometer (slit width corresponds to 10 nm), the intensity of probe pulse is recorded by photomultiplier (PMT) and lock-in amplifier. The objective we use in our experiments is 100× with NA = 0.90. Probe and pump pulse are focused at the sample with diameters of about 1 and 2 μm, respectively (we did not use full N.A. to avoid damage on the samples).

Deconvolution Process. The transient absorption signal of MoS_2 monolayer is from MoS_2 B-exciton probing and its curve rises instantaneously after the pump pulse excitation. Therefore, we can reproduce the dynamics curve of MoS_2 monolayer by a rapid rise curve (intrinsic MoS_2 transient absorption) and the instrument response function. From our fitting, the time scale of our instrument response is about 150 fs. Then, with the same instrument response function for time convolution, we reproduce the experimentally observed transient absorption signal in the heterostructure with a rise time around 90 fs, corresponding to the charge transfer time.

STEM Characterization. Annular dark-field (ADF) imaging was conducted by a probe-corrected scanning transmission electron microscope (FEI Titan G2 80−200 ChemiSTEM) operated at an acceleration voltage of 200 kV. In addition, the beam convergence angle was set to be 21.4 mrad with a probe current of 100−150 pA. Energy-dispersive X-ray spectroscopy (Bruker Super-X) integrated in STEM was utilized for the X-ray collection.

DFT Calculations. The excited state real-time TDDFT simulations were carried out with our developed time-dependent *ab initio* package TDAP based on SIESTA.[42] We used pseudopotentials of the Troullier-Martins type, the PBE exchange-correlation functional,[43] and a local basis set of double-ζ polarized (DZP) orbitals. Supercells in rectangle shape containing 108 atoms in the supercells for AA and AB stackings were used to model MoS_2/WS_2 heterostructures while a rhombus supercell with 126 atoms was used for the twist heterostructure with a relative angle of 38°. We have shown these models are enough to simulate the MoS_2/WS_2 heterostructures.[20] Electron−hole interaction and electron−phonon effects were naturally included in our methods. Although PBE functional usually underestimates the bandgaps, it is accurate enough to describe the spatial distribution of electronic states and the state couplings, which are crucial in our dynamic simulations. In addition, very similar band structures based on PBE functional and HSE06 functional are obtained (Supplementary Figure S7). Supercells in rectangle shape containing 108 atoms in the supercells were used to model bilayers with a single k-point for integration in the Brillouin zone and the states relative to the photoexcited states especially at K point in the first Brillouin zone are approximately folded to the supercells. The time step of all simulations was set to be 0.05 fs. Electron−hole (exciton effect) interaction and electron−phonon effects were naturally included in our methods.[42] The initial velocities of ions were assigned according to the equilibrium Boltzmann−Maxwell distribution at a given temperature of 77 and 350 K. We obtain no difference in the conclusion for the two temperatures. It should be noted that some energy levels in the supercells we used may be degenerate, so states with similar energy and spatial distributions have been checked in the following dynamic simulations to ensure the reliability of our results.

ASSOCIATED CONTENT

Ⓢ Supporting Information

The Supporting Information is available free of charge on the ACS Publications website at DOI: 10.1021/acsnano.7b04541.

Optical characterization of MoS_2/WS_2 heterostructures; Polarization dependent low-frequency Raman spectra of MoS_2/WS_2 heterostructures; Charge transfer time of MoS_2/WS_2 bilayers with different stacking configurations; Transient absorption spectra of CVD grown MoS_2/WS_2 bilayers probed at temperature of 77 K; High-symmetry stacking configurations of MoS_2/WS_2 bilayers; TDDFT calculations of charge transfer in

MoS$_2$/WS$_2$ bilayers with different interlayer sliding distance; Band structures of MoS$_2$/WS$_2$ bilayer in AB-2H stacking; More details on calculations (PDF)

AUTHOR INFORMATION

Corresponding Authors
*E-mail: chhjin@zju.edu.cn.
*E-mail: kebinshi@pku.edu.cn.
*E-mail: khliu@pku.edu.cn.

ORCID
Jin Zhang: 0000-0001-7830-3464
Liying Jiao: 0000-0002-6576-906X
Sheng Meng: 0000-0002-1553-1432
Kaihui Liu: 0000-0002-8781-2495

Author Contributions
∇Z.J., H.H., J.Z., and Q.Z. contributed equally to this work

Notes
The authors declare no competing financial interest.

REFERENCES

(1) Geim, A. K.; Grigorieva, I. V. Van der Waals Heterostructures. *Nature* **2013**, *499*, 419−425.

(2) Yu, W. J.; Liu, Y.; Zhou, H. L.; Yin, A. X.; Li, Z.; Huang, Y.; Duan, X. F. Highly Efficient Gate-Tunable Photocurrent Generation in Vertical Heterostructures of Layered Materials. *Nat. Nanotechnol.* **2013**, *8*, 952−958.

(3) Lee, C. H.; Lee, G. H.; van der Zande, A. M.; Chen, W. C.; Li, Y. L.; Han, M. Y.; Cui, X.; Arefe, G.; Nuckolls, C.; Heinz, T. F.; Guo, J.; Hone, J.; Kim, P. Atomically Thin p-n Junctions with van der Waals Heterointerfaces. *Nat. Nanotechnol.* **2014**, *9*, 676−681.

(4) Rivera, P.; Seyler, K. L.; Yu, H. Y.; Schaibley, J. R.; Yan, J. Q.; Mandrus, D. G.; Yao, W.; Xu, X. D. Valley-Polarized Exciton Dynamics in a 2D Semiconductor Heterostructure. *Science* **2016**, *351*, 688−691.

(5) Jin, C.; Kim, J.; Suh, J.; Shi, Z.; Chen, B.; Fan, X.; Kam, M.; Watanabe, K.; Taniguchi, T.; Tongay, S.; Zettl, A.; Wu, J.; Wang, F. Interlayer Electron-Phonon Coupling in WSe$_2$/hBN Heterostructures. *Nat. Phys.* **2017**, *13*, 127−131.

(6) Mak, K. F.; Lee, C.; Hone, J.; Shan, J.; Heinz, T. F. Atomically Thin MoS$_2$: A New Direct-Gap Semiconductor. *Phys. Rev. Lett.* **2010**, *105*, 136805.

(7) Splendiani, A.; Sun, L.; Zhang, Y. B.; Li, T. S.; Kim, J.; Chim, C. Y.; Galli, G.; Wang, F. Emerging Photoluminescence in Monolayer MoS$_2$. *Nano Lett.* **2010**, *10*, 1271−1275.

(8) Komsa, H. P.; Krasheninnikov, A. V. Electronic Structures and Optical Properties of Realistic Transition Metal Dichalcogenide Heterostructures from First Principles. *Phys. Rev. B: Condens. Matter Mater. Phys.* **2013**, *88*, 085318.

(9) Kang, J.; Tongay, S.; Zhou, J.; Li, J. B.; Wu, J. Q. Band Offsets and Heterostructures of Two-Dimensional Semiconductors. *Appl. Phys. Lett.* **2013**, *102*, 012111.

(10) Rivera, P.; Schaibley, J. R.; Jones, A. M.; Ross, J. S.; Wu, S. F.; Aivazian, G.; Klement, P.; Seyler, K.; Clark, G.; Ghimire, N. J.; Yan, J. Q.; Mandrus, D. G.; Yao, W.; Xu, X. D. Observation of Long-Lived Interlayer Excitons in Monolayer MoSe$_2$-WSe$_2$ Heterostructures. *Nat. Commun.* **2015**, *6*, 6242.

(11) Chiu, M. H.; Zhang, C. D.; Shiu, H. W.; Chuu, C. P.; Chen, C. H.; Chang, C. Y. S.; Chen, C. H.; Chou, M. Y.; Shih, C. K.; Li, L. J. Determination of Band Alignment in the Single-Layer MoS$_2$/WS$_2$ Heterojunction. *Nat. Commun.* **2015**, *6*, 7666.

(12) Hong, X. P.; Kim, J.; Shi, S. F.; Zhang, Y.; Jin, C. H.; Sun, Y. H.; Tongay, S.; Wu, J. Q.; Zhang, Y. F.; Wang, F. Ultrafast Charge Transfer in Atomically Thin MoS$_2$/WS$_2$ Heterostructures. *Nat. Nanotechnol.* **2014**, *9*, 682−686.

(13) Ceballos, F.; Bellus, M. Z.; Chiu, H. Y.; Zhao, H. Ultrafast Charge Separation and Indirect Exciton Formation in a MoS$_2$-MoSe$_2$ van der Waals Heterostructure. *ACS Nano* **2014**, *8*, 12717−12724.

(14) Chen, H. L.; Wen, X. W.; Zhang, J.; Wu, T. M.; Gong, Y. J.; Zhang, X.; Yuan, J. T.; Yi, C. Y.; Lou, J.; Ajayan, P. M.; Zhuang, W.; Zhang, G. Y.; Zheng, J. R. Ultrafast Formation of Interlayer Hot Excitons in Atomically Thin MoS$_2$/WS$_2$ Heterostructures. *Nat. Commun.* **2016**, *7*, 12512.

(15) Ceballos, F.; Ju, M. G.; Lane, S. D.; Zeng, X. C.; Zhao, H. Highly Efficient and Anomalous Charge Transfer in van der Waals Trilayer Semiconductors. *Nano Lett.* **2017**, *17*, 1623−1628.

(16) Zhu, H.; Wang, J.; Gong, Z.; Kim, Y. D.; Hone, J.; Zhu, X.-Y. Interfacial Charge Transfer Circumventing Momentum Mismatch at Two-Dimensional van der Waals Heterojunctions. *Nano Lett.* **2017**, *17*, 3591−3598.

(17) Zhu, X. Y.; Monahan, N. R.; Gong, Z. Z.; Zhu, H. M.; Williams, K. W.; Nelson, C. A. Charge Transfer Excitons at van der Waals Interfaces. *J. Am. Chem. Soc.* **2015**, *137*, 14230−14230.

(18) Long, R.; Prezhdo, O. V. Quantum Coherence Facilitates Efficient Charge Separation at a MoS$_2$/MoSe$_2$ van der Waals Junction. *Nano Lett.* **2016**, *16*, 1996−2003.

(19) Wang, H.; Bang, J.; Sun, Y. Y.; Liang, L. B.; West, D.; Meunier, V.; Zhang, S. B. The Role of Collective Motion in the Ultrafast Charge Transfer in van der Waals Heterostructures. *Nat. Commun.* **2016**, *7*, 11504.

(20) Zhang, J.; Hong, H.; Lian, C.; Ma, W.; Xu, X. Z.; Fu, H. X.; Liu, K. H.; Meng, S. Interlayer-State-Coupling Dependent Ultrafast Charge Transfer in MoS$_2$/WS$_2$ Bilayers. *Adv. Sci.* **2017**, *4*, 1700086.

(21) Liu, K. H.; Zhang, L. M.; Cao, T.; Jin, C. H.; Qiu, D. A.; Zhou, Q.; Zettl, A.; Yang, P. D.; Louie, S. G.; Wang, F. Evolution of Interlayer Coupling in Twisted Molybdenum Disulfide Bilayers. *Nat. Commun.* **2014**, *5*, 4966.

(22) Hong, H.; Liu, C.; Cao, T.; Jin, C. H.; Wang, S. X.; Wang, F.; Liu, K. H. Interfacial Engineering of van der Waals Coupled 2D Layered Materials. *Adv. Mater. Interfaces* **2017**, *4*, 1601054.

(23) Zhang, Q.; Xiao, X.; Zhao, R. Q.; Lv, D. H.; Xu, G. C.; Lu, Z. X.; Sun, L. F.; Lin, S. Z.; Gao, X.; Zhou, J.; Jin, C. H.; Ding, F.; Jiao, L. Y. Two-Dimensional Layered Heterostructures Synthesized from Core-Shell Nanowires. *Angew. Chem., Int. Ed.* **2015**, *54*, 8957−8960.

(24) Gong, Y. J.; Lin, J. H.; Wang, X. L.; Shi, G.; Lei, S. D.; Lin, Z.; Zou, X. L.; Ye, G. L.; Vajtai, R.; Yakobson, B. I.; Terrones, H.; Terrones, M.; Tay, B. K.; Lou, J.; Pantelides, S. T.; Liu, Z.; Zhou, W.; Ajayan, P. M. Vertical and in-Plane Heterostructures from WS$_2$/MoS$_2$ Monolayers. *Nat. Mater.* **2014**, *13*, 1135−1142.

(25) Zhang, J.; Wang, J. H.; Chen, P.; Sun, Y.; Wu, S.; Jia, Z. Y.; Lu, X. B.; Yu, H.; Chen, W.; Zhu, J. Q.; Xie, G. B.; Yang, R.; Shi, D. X.; Xu, X. L.; Xiang, J. Y.; Liu, K. H.; Zhang, G. Y. Observation of Strong Interlayer Coupling in MoS$_2$/WS$_2$ Heterostructures. *Adv. Mater.* **2016**, *28*, 1950−1956.

(26) van der Zande, A. M.; Huang, P. Y.; Chenet, D. A.; Berkelbach, T. C.; You, Y. M.; Lee, G. H.; Heinz, T. F.; Reichman, D. R.; Muller, D. A.; Hone, J. C. Grains and Grain Boundaries in Highly Crystalline Monolayer Molybdenum Disulphide. *Nat. Mater.* **2013**, *12*, 554−561.

(27) Zhou, X.; Cheng, J. X.; Zhou, Y. B.; Cao, T.; Hong, H.; Liao, Z. M.; Wu, S. W.; Peng, H. L.; Liu, K. H.; Yu, D. P. Strong Second-Harmonic Generation in Atomic Layered GaSe. *J. Am. Chem. Soc.* **2015**, *137*, 7994−7997.

(28) Zhao, Y. Y.; Luo, X.; Li, H.; Zhang, J.; Araujo, P. T.; Gan, C. K.; Wu, J.; Zhang, H.; Quek, S. Y.; Dresselhaus, M. S.; Xiong, Q. H. Interlayer Breathing and Shear Modes in Few-Trilayer MoS$_2$ and WSe$_2$. *Nano Lett.* **2013**, *13*, 1007−1015.

(29) Zhang, X.; Han, W. P.; Wu, J. B.; Milana, S.; Lu, Y.; Li, Q. Q.; Ferrari, A. C.; Tan, P. H. Raman Spectroscopy of Shear and Layer Breathing Modes in Multilayer MoS$_2$. *Phys. Rev. B: Condens. Matter Mater. Phys.* **2013**, *87*, 115413.

(30) Lui, C. H.; Ye, Z. P.; Ji, C.; Chiu, K. C.; Chou, C. T.; Andersen, T. I.; Means-Shively, C.; Anderson, H.; Wu, J. M.; Kidd, T.; Lee, Y. H.; He, R. Observation of Interlayer Phonon Modes in van der Waals Heterostructures. *Phys. Rev. B: Condens. Matter Mater. Phys.* **2015**, *91*, 165403.

(31) Yan, J. X.; Xia, J.; Wang, X. L.; Liu, L.; Kuo, J. L.; Tay, B. K.; Chen, S. S.; Zhou, W.; Liu, Z.; Shen, Z. X. Stacking-Dependent Interlayer Coupling in Trilayer MoS$_2$ with Broken Inversion Symmetry. *Nano Lett.* **2015**, *15*, 8155−8161.

(32) Huang, S. X.; Liang, L. B.; Ling, X.; Puretzky, A. A.; Geohegan, D. B.; Sumpter, B. G.; Kong, J.; Meunier, V.; Dresselhaus, M. S. Low-Frequency Interlayer Raman Modes to Probe Interface of Twisted Bilayer MoS$_2$. *Nano Lett.* **2016**, *16*, 1435−1444.

(33) Kozawa, D.; Carvalho, A.; Verzhbitskiy, I.; Giustiniano, F.; Miyauchi, Y.; Mouri, S.; Neto, A. H. C.; Matsuda, K.; Eda, G. Evidence for Fast Interlayer Energy Transfer in MoSe$_2$/WS$_2$ Heterostructures. *Nano Lett.* **2016**, *16*, 4087−4093.

(34) Zhang, C. D.; Chuu, C. P.; Ren, X. B.; Li, M. Y.; Li, L. J.; Jin, C. H.; Chou, M. Y.; Shih, C. K. Interlayer Couplings, Moire patterns, and 2D Electronic Superlattices in MoS$_2$/WSe$_2$ Hetero-Bilayers. *Sci. Adv.* **2017**, *3*, e1601459.

(35) Alden, J. S.; Tsen, A. W.; Huang, P. Y.; Hovden, R.; Brown, L.; Park, J.; Muller, D. A.; McEuen, P. L. Strain Solitons and Topological Defects in Bilayer Graphene. *Proc. Natl. Acad. Sci. U. S. A.* **2013**, *110*, 11256−11260.

(36) Butz, B.; Dolle, C.; Niekiel, F.; Weber, K.; Waldmann, D.; Weber, H. B.; Meyer, B.; Spiecker, E. Dislocations in Bilayer Graphene. *Nature* **2014**, *505*, 533−537.

(37) Woods, C. R.; Britnell, L.; Eckmann, A.; Ma, R. S.; Lu, J. C.; Guo, H. M.; Lin, X.; Yu, G. L.; Cao, Y.; Gorbachev, R. V.; Kretinin, A. V.; Park, J.; Ponomarenko, L. A.; Katsnelson, M. I.; Gornostyrev, Y. N.; Watanabe, K.; Taniguchi, T.; Casiraghi, C.; Gao, H. J.; Geim, A. K.; Novoselov, K. S. Commensurate-Incommensurate Transition in Graphene on Hexagonal Boron Nitride. *Nat. Phys.* **2014**, *10*, 451−456.

(38) Liu, Z.; Amani, M.; Najmaei, S.; Xu, Q.; Zou, X. L.; Zhou, W.; Yu, T.; Qiu, C. Y.; Birdwell, A. G.; Crowne, F. J.; Vajtai, R.; Yakobson, B. I.; Xia, Z. H.; Dubey, M.; Ajayan, P. M.; Lou, J. Strain and Structure Heterogeneity in MoS$_2$ Atomic Layers Grown by Chemical Vapour Deposition. *Nat. Commun.* **2014**, *5*, 5246.

(39) Zhu, Z. Y.; Cheng, Y. C.; Schwingenschlogl, U. Giant Spin-Orbit-Induced Spin Splitting in Two-Dimensional Transition-Metal Dichalcogenide Semiconductors. *Phys. Rev. B: Condens. Matter Mater. Phys.* **2011**, *84*, 153402.

(40) Peng, B.; Zhang, H.; Shao, H. Z.; Xu, Y. C.; Zhang, X. C.; Zhu, H. Y. Thermal Conductivity of Monolayer MoS$_2$, MoSe$_2$, and WS$_2$: Interplay of Mass Effect, Interatomic Bonding and Anharmonicity. *RSC Adv.* **2016**, *6*, 5767−5773.

(41) Runge, E.; Gross, E. K. U. Density-Functional Theory for Time-Dependent Systems. *Phys. Rev. Lett.* **1984**, *52*, 997−1000.

(42) Meng, S.; Kaxiras, E. Real-Time, Local Basis-Set Implementation of Time-Dependent Density Functional Theory for Excited State Dynamics Simulations. *J. Chem. Phys.* **2008**, *129*, 054110.

(43) Perdew, J. P.; Burke, K.; Ernzerhof, M. Generalized Gradient Approximation Made Simple. *Phys. Rev. Lett.* **1996**, *77*, 3865.